CAAP Quarterly Report

[12/26/2025]

Project Name: "All-in-One Multifunctional Cured-In-Place Structural Liner for Rehabilitating of Aging Cast Iron Pipelines"

Contract Number: 693JK32250009CAAP

Prime University: North Dakota State University

Prepared By: [Ying Huang, ying.huang@ndsu.edu, 701-231-7651]

Reporting Period: [09/27/2025– 12/27/2025]

Project Activities for Reporting Period:

In the 12th quarterly report, Tasks 2, 3, 4, and 5 were carried out as proposed. During the current reporting period (Q13), the research team continued to make steady progress on these tasks. Key accomplishments from this quarter are summarized in the sections that follow.

Task 2.1 Preparation of Vitrimer Epoxy Resins, Characterization, and Optimization of Processing and Curing Conditions (99%): During the past quarter, the research team (Dr. Long Jiang and Austin Knight, Ph.D. student at NDSU), developed new formulation strategies to improve thermal performance by incorporating a short-chain aliphatic crosslinker (DFAAl). After optimizing the transesterification catalyst (TEC) and hydroxyl solvent (HS) contents, the viscoelastic behavior of the DFAAl formulation was evaluated. Based on these results, formulations with longer-chain crosslinkers (DFAAl2 and DFAAl3) were also assessed to examine the effect of crosslinker length on material response. Key findings are summarized below:

(1) Viscoelastic Characterization of the DFAAl Formulation: Initial testing showed that the difunctional aliphatic crosslinker (DFAAl) adhesive, when only UV-cured, exhibited shrinkage and excessive hardening above 100°C. To address this issue, all samples were post-cured at 120°C for 2 hours after UV curing, and subsequent testing was limited to temperatures below 100°C where applicable. Dynamic mechanical analysis (DMA) measured the glass transition temperature (Tg) as 107.9°C (Figure 1a). A dynamic strain sweep was conducted to identify the linear viscoelastic region (LVER) for stress relaxation testing. A 10% drop in storage modulus occurred at 0.13% strain, while stress relaxation tests were performed at 0.5% strain, corresponding to a 30% reduction in storage modulus (Figure 1b). Stress relaxation tests at 60, 70, 80, and 90°C were used to estimate the topology freezing temperature (Tv), defined as the temperature at which viscosity reaches 10^{12} Pa·s. Regression analysis yielded a Tv of 43.0°C, consistent with the strong self-healing behavior observed in the previous quarter (Figures 1c and 1d). This Tv is notably lower than the value obtained from prior dilatometry measurements, prompting repeat dilatometry using post-cured samples to resolve the discrepancy.

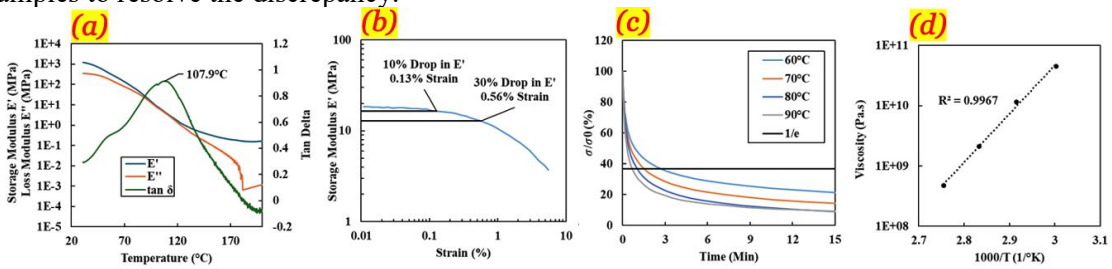

Figure 1. The (a) DMA, (b) dynamic strain sweep, (c) stress relaxation, and (d) viscosity regression of the DFAAl formulation.

(2) Addition of Longer Chain Adduct Crosslinkers: Longer-chain aliphatic crosslinkers (DFAAl2 and DFAAl3) were synthesized and formulated with 100 parts RDMA and 20 parts TEC to compare their dilatometry behavior with DFAAr and DFAAl formulations (Figure 2). To reduce formulation preparation time, the mixing protocol was modified from 24 hours of magnetic stirring at 500 rpm to five cycles of 30 s sonication at 40% amplitude followed by 1 minute of vortex mixing. This approach improved TEC dispersion but caused the more viscous DFAAr2 and DFAAr3 formulations to form pastes that could not be cured or tested. Dilatometry results for the tested formulations indicate that DFAAr and DFAAl exhibit similar glass transition temperature (Tg), topology freezing temperature (Tv), and maximum strain, with DFAAl showing slightly improved performance across all metrics. In contrast, DFAAl2 and DFAAl3 displayed progressively lower Tg and Tv with increasing crosslinker length, along with a substantial reduction in maximum strain compared to the short-chain formulations. The reduced strain capacity of the longer-chain crosslinkers requires further investigation, while future characterization efforts will focus on the short-chain systems.

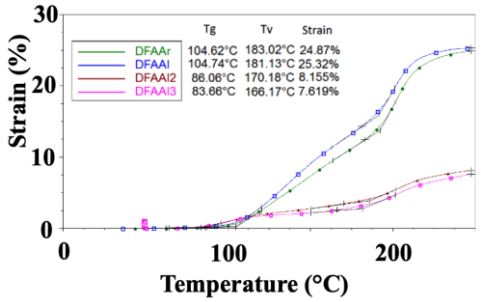

Figure 2. Dilatometry results at 100kPa at 3°C/min for formulations containing 100-RDMA and 20-TEC and DFAAr, DFAAl, DFAAl2, and DFAAl3

Task 3.3 Reducing the Permeability and Investigating the Interfacial Bonding Chemical Analysis (95%): In previous work, the research team (Dr. Liangliang Huang and Hao Yuan, Ph.D. student at the University of Oklahoma) performed a comprehensive evaluation of the with newly developed scaled up vitrimer model was carried out. During this reporting period, evaluation of the vitrimer system continued, with focus on the reaction probability for the self-healing reaction. To this end, longer simulation times were employed to capture the time-dependent recovery of mechanical properties.

(1) Reaction Probability for Self-healing Polymer: The dynamic bond exchange in the BisGMA:2-HEMA vitrimer is modeled using a temperature dependent probability of the dynamic bond reaction. The consideration of achieving a gradual increase in the response rate in the vicinity of the transition temperature, T_g, is undertaken. In Figure 3, based on the calculated reaction probability, the number of reactions for vitrimers at different temperatures is presented in Figure 3. No bond exchange reactions are observed below 399 K. Once the temperature exceeds the reaction threshold, bond exchange events begin to occur. Between 400 K and 450 K, the number of reactions remains relatively steady. This plateau is attributed to the ongoing transition of the vitrimer from the glassy state to the rubbery or melt-like state, during which significant steric hindrance limits the mobility and interaction of polymer chains. As the temperature increases further, chain dynamics become more active and the system exhibits greater free volume, thereby facilitating a higher frequency of bond exchange reactions.

(2) Self-healing Behavior Through Varied Temperatures: As presented in Figure 4, at 300 K, no vitrimer reaction occurs. The vitrimer chains merely entangle through thermal motion, resulting in a very limited self-healing capability. After only 0.1 ns of healing, the Young's modulus remains extremely low, corresponding to a healing efficiency of approximately 31.6%. With increasing healing time, the recovery of mechanical properties initially proceeds rapidly and then gradually approaches saturation. The healing efficiency reaches about 69% at approximately 2 ns and further increases to 75.5% after 5 ns of healing. When the temperature reaches 400 K or higher, the vitrimer's recovery can reach 98% after 5 ns of self-healing.

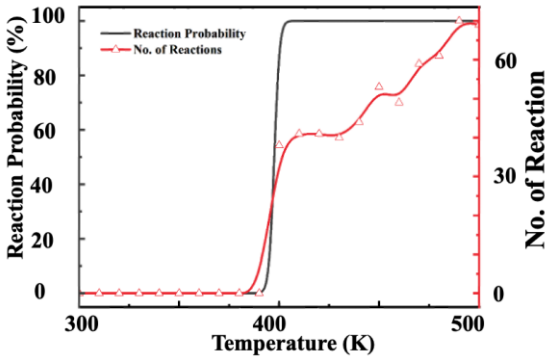

Figure 3. Reaction probability in self-healing polymer at varied temperatures.

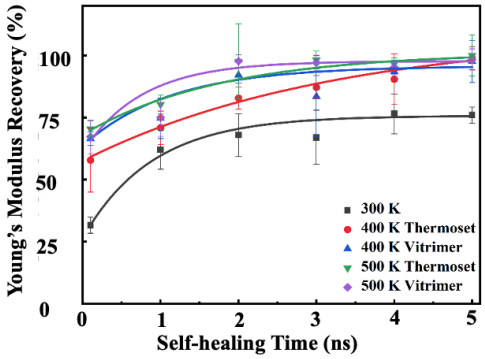

Figure 4. Evolution of Young's modulus as a function of healing time for vitrimer systems under different conditions.

Task 3.4 Finite Element Numerical Analysis to Guide the Design of the Developed High-performance Healable CIPP Structural Liner (98%): During this reporting period, the research team (Dr. Chengcheng Tao, Junyi Duan, and Yizhou Lin, Ph.D. students from Purdue University) developed finite element analysis (FEA) to evaluate the mechanical behavior of epoxy-based nanocomposite materials used in the liner adhesive layer. The results are summarized below:

(1) Finite Element Analysis of Tensile Properties of Nanocomposite Materials in Adhesive Layer: In this task, FEA is performed to study epoxy-based nanocomposites reinforced by nanodiamonds (ND), carbon nanotubes (CNT), and graphene nanoplatelets (GNP). RVE modeling is used to simulate stress-strain behavior under tensile loading, enabling the translation of microscopic interactions between nanoparticles and the epoxy matrix into macroscopic properties. The RVEs are generated with randomly distributed nanoparticles to better represent real microstructures. Epoxy and three types of nanoparticles (0D ND, 1D CNT, 2D GNP) are assigned. Fibers are randomly positioned and oriented using spherical coordinates, ensuring they stay within the RVE domain. Figure 5 (a), (b), and (c) illustrate representative random distributions of nanoparticles from the RVE generation process in Abaqus. Figure 6 presents the finite element simulation results of epoxy nanocomposites reinforced with randomly distributed nanoparticles at weight fractions of 0.5%, 1.0%, and 2.0%, respectively. The results show that the addition of nanoparticle enhances tensile strength. The enhancement is influenced by both filler type and orientation, where ND demonstrates the least effect, CNT demonstrates moderate effect,

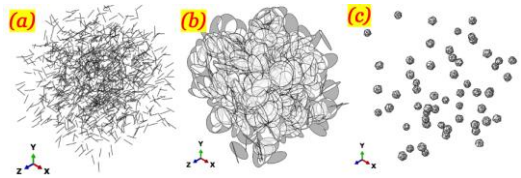

Figure 5. Representative random dispersion of nanoparticles: (a) ND, (b) CNT, and (c) GNP.

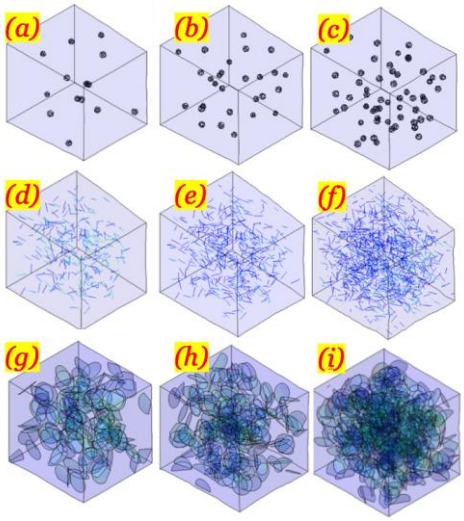

Figure 6. FEA models of (a-c) ND, (d-f) CNT, and (g-i) GNP at weight fractions of 0.5%, 1.0%, and 2.0%.

while GNP demonstrates the strongest effect. Variability in tensile strength between RVEs is small for ND but larger for CNT and GNP due to their directional geometry.

Task 4.1 Development of Embedded Distributed Fiber Optic Sensors for Self-sensing Structural Liner (99%), and **Task 4.2** Investigating the Load Transfer between Layers of the CIPP Liner and the Cast-iron Substrate (90%): During this reporting period, the research team (Dr. Ying Huang, Dr. Xingyu Wang and Dr. Chengcheng Tao, and Huaixiao Yan, Ph.D. student from Purdue University) investigated efficient deployment strategies for distributed fiber optic sensing (DFOS) in the smart-liner system. The sensor layout optimization was informed by results from previous buckling experiments and focused on developing a method that enables the smart liner to capture structural deformation while minimizing the required number of DFOS sensors. Key findings from this study are summarized below:

(1) Optimization of Sensor Location and Layout: The radial basis function (RBF) method was employed to reconstruct the strain field, as it demonstrated the highest accuracy among the evaluated approaches. Strain gradients were then calculated from the reconstructed field to inform sensor placement. Figure 7 compares the spatial distribution of selected sensor locations under four different layout strategies, where the strain-gradient field is shown in blue and proposed sensor locations are overlaid as color-coded markers. The integrated strategy combines the strengths of three methods, weighted k-means, hotspot thresholding, and DBSCAN clustering, to achieve a more balanced sensor layout. Candidate locations from each method are treated as a voting pool, and final sensor sites are selected to ensure coverage of major high-gradient regions, inclusion of peak gradient locations, and adequate spatial distribution. All three methods were applied independently to generate candidate sets, which were then merged and refined. Building on these results, a density-based routing method was introduced to significantly improve the practical deployability of the selected sensor locations.

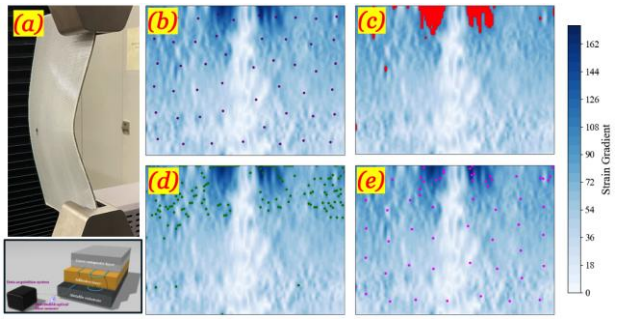

Figure 7. (a) Buckling test of liner system; and critical location by different methods; (b) K-Means weighted clustering; (c) High-gradient hotspots; (d) DBSCAN clustering; (e) Integrated strategy.

(2) Suggested Sensor Layout for Buckling: To evaluate the practicality and performance of different DFOS layout strategies, a spatial density-based framework was implemented to generate sensing paths in horizontal, vertical, and diagonal directions. Figure 8(a) shows the resulting DFOS configurations for a plate divided into six uniform regions. Forty candidate points from the integrated strategy are shown in blue, with DFOS lines overlaid in red (horizontal), green (vertical), and orange (diagonal). This approach provides effective coverage of high-strain regions while limiting routing complexity. Figure 8(b) presents a radar chart comparing the three layouts across six standardized performance metrics. Optimal layouts minimize average distance, total length, and number of paths, while maximizing minimum distance, coverage ratio, and distribution standard deviation. Because candidate points are concentrated in the upper-middle region due to localized buckling, this spatial bias influences the results. The horizontal layout achieves the highest sensing accuracy but suffers from tight spacing that complicates installation. The vertical layout offers the best balance between performance and deployability, while the diagonal layout provides the greatest installation flexibility at the expense of reduced coverage and sensing resolution.

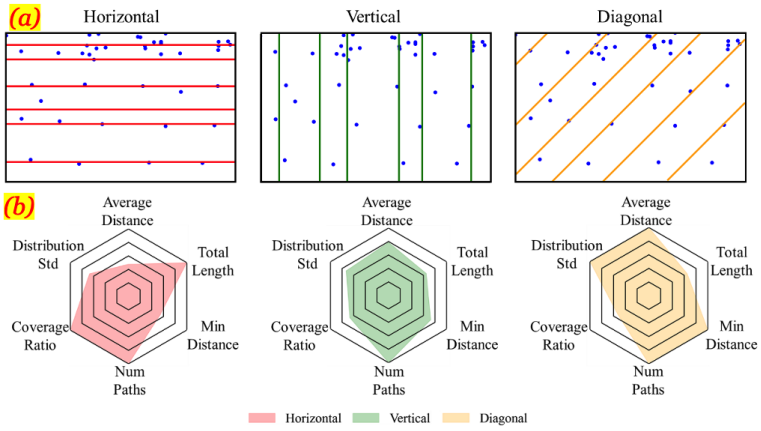

Figure 8. (a) Suggested DFOS layout in three directions; (b) Evaluate metrics of the DFOS layout.

Task 5.1 Development of CIPP Liner Risk Index for the Pipeline Integrity Management Enhanced by AI Algorithms (80%) and **Task 5.2** Full-size laboratory testing for system validation (50%): During this period, the research team (Dr. Chengcheng Tao, Yizhou Lin, and Jiannan Ding, Ph.D. students from Purdue University) developed models to predict remaining useful life and to simulate a full-scale pipe with an integrated liner system. The key results are outlined below:

(1) Remaining Useful Life Prediction of Pipelines: To evaluate the remaining useful life (RUL) of pipelines, this task develops a framework for assessing dented pipelines by integrating dent-depth- and strain-based severity criteria with fatigue analysis under realistic internal pressure fluctuations. This approach provides a more accurate evaluation of dent severity and its impact on long-term serviceability, extending beyond the static 6% OD criterion commonly used in current standards. Figure 9 illustrates the RUL assessment and fitness-for-service decision framework used to determine whether a dented pipeline can safely continue operation over its intended service life. The process involves the following steps:

a. Data collection and condition characterization. In this step, comprehensive data are gathered regarding the asset's physical condition, operating history, and environmental exposure. This includes material properties, geometrical features, defect characteristics (e.g., size, depth), and loading conditions (e.g., internal pressure cycles).

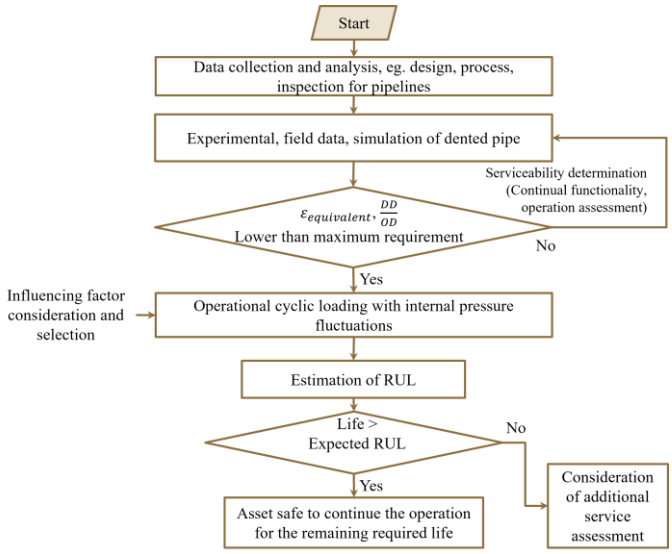

Figure 9. Framework of RUL assessment and fitness-for-service decision.

b. Definition of operational and service requirements. The intended future service duration, performance expectations, and applicable safety or regulatory standards are clearly defined. This may include pressure thresholds, and any limits imposed by industrial codes.

c. Preliminary structural assessment. An initial evaluation is performed to screen the asset's current condition against allowable limits or screening criteria. This may involve simplified methods

such as empirical formulas, safety factors, or rule-based compliance checks to determine whether the asset obviously meets or fails the requirements.

d. Criteria compliance check. A decision is made on whether the asset satisfies the preliminary screening criteria. If the criteria are not met, the process loops back for either re-assessment with improved data or refinement of the evaluation model. If the criteria are met, the analysis proceeds to more detailed modeling.
e. Detailed structural integrity evaluation. Advanced analysis using finite element modeling is conducted to quantify stress and strain distributions, plastic deformation under actual and projected loading conditions.
f. Execution of life prediction or degradation models. Based on the detailed evaluation, established models are employed to predict the RUL. In this study, fatigue analysis is used to get the estimated cycle.
g. Comparison with required remaining life. The predicted RUL is then compared against the predefined operational requirement. This determines if the asset can sustain the expected service duration without exceeding acceptable risk levels.
h. Sufficiency of RUL. A second critical decision is made in this step. If the predicted RUL is sufficient, the asset is deemed safe to continue operation for the required duration. If not, the process proceeds to 9).
i. Consideration of additional assessment or mitigation measures. If the current state does not meet the operational requirements, further assessments may be necessary. These could involve inspection techniques, material testing, or consideration of repair, reinforcement, or operational derating.

(2) Finite Element Analysis of the Pipe-Liner System: A full-scale pipe–liner system with corrosion defects was developed to support the pipe–liner experimental program. A parametric corrosion–fatigue assessment was then conducted using a cast iron pipeline model with a diameter of 600 mm and a wall thickness of 15.9 mm. Cast iron was selected due to its historical use in pipeline systems and its susceptibility to corrosion under service conditions. To investigate the coupled effects of corrosion and geohazard-induced deformation, two comparative configurations were considered: a reference model without corrosion and a model with surface pitting corrosion. To systematically capture degradation behavior, 28 finite element models were developed with controlled corrosion parameters, including mean pit depths ranging from 0 to 12.7 mm, pit counts following an exponential growth trend, and pit diameters defined by the relationship pitting depth = 0.136 × pitting diameter. Figure 10 presents representative FEA geometries of the corroded pipe–liner models, including overall and cross-sectional views. These parameters were selected to simulate progressive damage over service time and to represent different stages of pipeline aging.

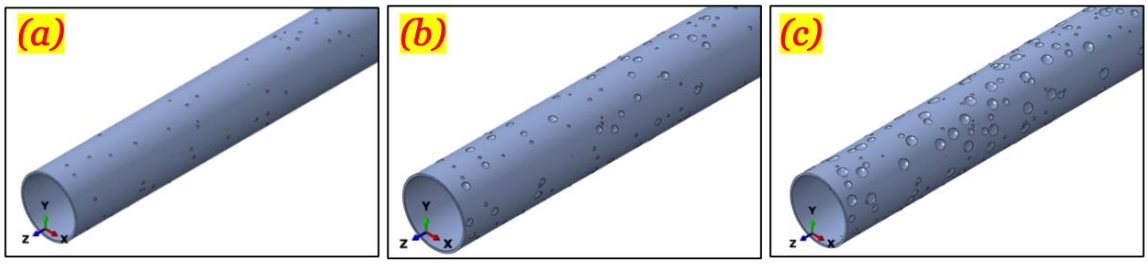

Model 1: # of defects = 42, average depth = 5 mm; average diameter = 36.7 mm.

Model 2: # of defects = 103, average depth = 8 mm, average diameter = 58.8 mm.

Model 3: # of defects = 175, average depth = 12.7mm, average diameter = 80.9 mm.

Figure 10. Geometric view of cast iron pipeline models with varying pitting corrosion depths. (a) Model 1, (b) Model 2, and (c) Model 3.

Project Financial Activities Incurred during the Reporting Period:

The cost breakdown during the reporting period according to the budget proposal is shown in Table 1.

Table 1. Cost breakdown

Category	Amount spent during Q13
Personnel	
Faculty	$0.00
Postdoc	$1,499.94
Students (RA and UR)	$12,900.23
Benefits	$887.53
Operating Expenses	
Travel	$0.00
Materials and Supplies	$0.00
Professional Development	$1,125.00
Recharge Center Fee	$865.50
Consultant Fee	$600.00
Subcontracts	$54,968.26
Indirect Costs	$7,566.02

Project Activities with Cost Share Partners:

The Match fund from NDSU for this project is coming from the tuition of the associated graduate students during their work on this project. During the reporting period (Q13), Zahoor Hussain (100%), Austin Knight (100%), and Tofatun Jannet (100%) were working on the project. The tuition for the three students during Q13 was estimated to be $12,520 at a rate of $463.73 per credit.

Project Activities with External Partners:

During this reporting period, George Ragula, our industry consultant, attended all the meetings with the research team.

Potential Project Risks:

No potential risks were noticed during this reporting period.

Future Project Work:

The research team will continue working on Tasks 2, 3, 4, and 5.

Potential Impacts on Pipeline Safety:

Results from the development of self-healing polymers demonstrated strong cut-healing performance across all formulations. Integration of the developed molecular dynamics models and finite-element nanocomposite simulations will enable a more comprehensive understanding and optimization of self-healing behavior based on simulation results. The optimized sensor layout strategy improves DFOS sensor deployment in the all-in-one liner system, achieving enhanced sensing performance while reducing sensor quantity and costs. The developed remaining useful life (RUL) prediction models enable improved estimation of pipeline service life and highlight the need for adaptive inspection scheduling. In addition, the developed full-scale pipe–liner system is designed to support full-scale experimental validation. Overall, the results demonstrate the potential applicability of the developed liner system to full-scale pipelines and provide guidance for optimizing cured-in-place pipe (CIPP) liner design and fabrication.